SIMULATING LUNAR APPROACH AND PINPOINT LANDINGS THROUGH ENHANCING DEMS AND REALSITIC IMAGE GENERATION

Iain Martin [(1)], Martin Dunstan [(1)], Manuel Sanchez-Gestido [(2)]

[(1)] University of Dundee, Dundee, DD1 4HN, United Kingdom, imartin@dundee.ac.uk
[(2)] Manuel Sanchez Gestido, ESTEC, ESA, Noordwijk, The Netherlands, manuel.sanchez.gestido@esa.int

ABSTRACT

Plans for future lunar exploration through both robotic and planned human controlled missions are defining increasingly stringent requirements for guidance of approach, surface relative navigation, and hazard detection, for pin-point landings on difficult terrain under contrasting illumination conditions. Autonomous GNC and hazard avoidance systems are continuing to be developed and validated to meet these mission requirements. This paper describes the creation of two representative lunar simulations to cover a pinpoint landing, utilising high-quality publicly available Digital Elevation Models and a long-distance approach over a hemisphere of the Moon. These are imported into the Planet and Asteroid Natural Scene Generation Utility, enhanced with representative terrain and small-scale features below the viable resolution of the DEMs, and high-frequency texture to obtain a large, high-resolution 3D model. Synthetic surface images are rendered with appropriate lighting and camera- distortion in real-time. These scenarios are not tailored for specific missions but are instead designed to be representative of potential missions which can be modified with different input data and generation parameters as required. Details are included of the imported DEMs, and the creation of the resolution enhanced models used to generate the images sequence including resolution and frame rates obtained of the simulated descents.

1 INTRODUCTION

Lunar exploration through both robotic and planned human controlled missions are being pursued through a variety of studies and missions from ESA, NASA and other space agencies. These missions are increasingly defining stringent requirements for guidance of approach, surface relative navigation and hazard detection for pin-point landings on difficult terrain under different illumination conditions. Autonomous GNC and hazard avoidance systems have been developed and extended over the past few decades [1] to attempt to meet current and future mission requirements, such as a pinpoint lunar landing near the South Pole region with rough terrain and large shadowed areas. While there is a large dataset of real images of lunar terrain, these are insufficient for training, testing and evaluating the proposed navigation systems. Synthetic imagery is a useful approach to augment the data required for testing and developing guidance systems for challenging mission scenarios, if it can be generated with realistically representative terrain with the required resolution, frame rate and lack of artefacts,

Generating simulated images to test navigation instruments at high speed with model resolution ranging from kilometres to centimetres is a challenging task due the large model sizes, the image resolution range and the requirement to support closed-loop testing in real or near-real time (i.e.

~10 Hz). We approach the synthetic image generation problem for lunar scenarios, through creating a multi-resolution model from synthetically enhancing DEMs with additional fractal terrain to increase the generic terrain resolution in high-resolution sections and then modifying the DEM through the addition of terrain features at higher resolutions than are defined in the original DEM [2]. This model is then rendered at high-frame rates including GPU-based camera model distortions to apply realistic camera noise and distortion in real-time to support closed loop test systems, as well as to generate the large volumes of data required to train machine learning GNC systems.

2 BACKGROUND

2.1 Lunar Missions

The European Space Agency (ESA) and the National Aeronautics and Space Administration (NASA) are both running current programmes to further lunar exploration and develop technologies for pinpoint landings, with the South Pole of the Moon an area of particular interest [3]. For example, the NASA Artemis programme is developing the Orion spacecraft, which includes a European Service Module, which intends to return humans to the Moon [4]. ESA have their own Lunar Lander programme to send a robotic explorer to the lunar surface to demonstrate key technologies and include a pinpoint landing on hazardous terrain near the South Pole [5]. The ESA Large Logistics Lander (Heracles) is intended to develop and prove the technologies for a variety of lunar missions including a sample return including a surface rover [6].

2.2 Autonomous guidance systems

To support the test, development and calibration of pinpoint landers, a combination of real and synthetic lunar imagery can be used to test and train the autonomous GNC systems. This is difficult to achieve using only real lunar images which are limited to the existing dataset, taken with particular illumination conditions and resolution so synthetic images have long been used in this field [7]. Established methods of generating synthetic lunar images under different lighting conditions include robotic cameras taking images of mocked up terrain and raytracing or rendering images from 3D models. The 3D models can be based on the most appropriate Digital Elevation Models (DEM) of the Moon which are data products from current and previous missions such as Lunar Reconnaissance Orbiter (LRO), Kaguya and the Chang'e series of missions. The highest quality lunar DEMs vary in range and resolution from global elevation datasets such as the combined LRO/Kaguya SLDEM with a maximum resolution of ~60 m per pixel at the equator [8] to higher resolution DEM products of local sections of around 5m per pixel from both the Lunar Orbiter Laser Altimeter (LOLA) instrument and derived from stereo images from the LRO Camera (LROC) and Narrow Angle Camera (NAC). However, features defined around the resolution limit of these DEMs are not generally clearly defined and this can cause difficulties when applying synthetic resolution enhancement techniques as is shown later in Section 4.3.

2.3 Image generation tools

A variety of tools have and are continuing to be developed to support the generation of synthetic and enhanced imagery to support GNC testing with different focuses and underlying technologies. For example, the Airbus proprietary software, SurRender [12], SIPSO (Space Imaging Simulator for Proximity Operations) [13] which used the Blender rendering engine and PANGU (Planet and Asteroid Natural Scene Generation Utility) [9] are all generalised tools that can be used to support a variety of image simulation scenarios.

3 PANGU Overview

PANGU has been designed to aid the testing and verification of a wide range of spacecraft missions by providing realistic simulations of onboard sensors including visual cameras, thermal cameras [10] and LiDAR instruments [9]. PANGU contains surface modelling and enhancement tools, a custom-designed visualisation tool based on GPU-rendering for high framerates, flexible integration options to interface with other simulators and a NAIF/SPICE interface which can be used where SPICE data is available such as to accurately simulate historical events or for future mission missions [9]. Terrain data such as surface DEMs and small body shape models can be imported in standard formats and enhanced into large, multi-resolution models to enable realistic approach and landing simulations from orbit to surface touch down. Artificial models can be generated for mission scenarios where real data is unavailable and spacecraft and rover models can be imported and included in simulations if appropriate. The image visualisation tool is a custom renderer that includes simulated camera distortion through the integrated, parameterizable GPU-based camera model.

To generate a sequence of synthetic lunar images for a specific mission in PANGU, the general approach taken is to select the most appropriate lunar DEM and import that into PANGU. Then identify the section or sections of the DEM that require resolution enhancement and specify the exact position and resolution increases required. For any significant resolution enhancement, we would add distributions of features such as craters, boulders or mounds that would not be clearly defined in the original DEM. In PANGU this can be done by specifying the size-density distributions (and age/decay distribution for craters) for that area from which a probability distribution can be defined for the size range of the additional features to add for each synthetic layer. These feature lists are defined as text files that can be edited or imported from another tool if required. The 3D position of each added synthetic feature is available in world coordinates as an available output from the model generation process to use for ground truth. To avoid the issue of partially-defined craters close to the limit of the DEM resolution, these can be replaced with synthetic alternatives but these need to be manually identified by the user using the surface modeller GUI tool. Albedo maps and textures can also be applied with feature-related albedo variations (such as dark or bright halo craters) being a recent additional feature.

The PANGU 3D lunar models described in this paper are based on the combined LRO/Kaguya SLDEM [8] with a maximum horizontal resolution of ~60m per pixel at the equator and a DEM derived from stereo images from the LRO Camera (LROC) and Narrow Angle Camera (NAC) with a resolution of 5m..

4 LANDING SITE OR SURFACE REOVER SCNARIO

The first scenario is a PANGU model suitable for simulating a landing site or a surface rover scenario, generated from a high-resolution DEM to demonstrate the simulation of a final approach and landing to a pre-selected target site.

4.1 LROC DEM

An example high-resolution LROC stereo DEM, NAC_DTM_A12LMAS_E039S3387.img, was obtained which covers (4.81172093N, 338.50996587E) to (3.05020714S, 338.97092643E) with a resolution of 5m and a reported precision error of 1.95m [15]. This DEM has 2790×10683 samples with 32-bit sample resolution with an equirectangular projection. An image showing this DEM is shown in Figure 1.

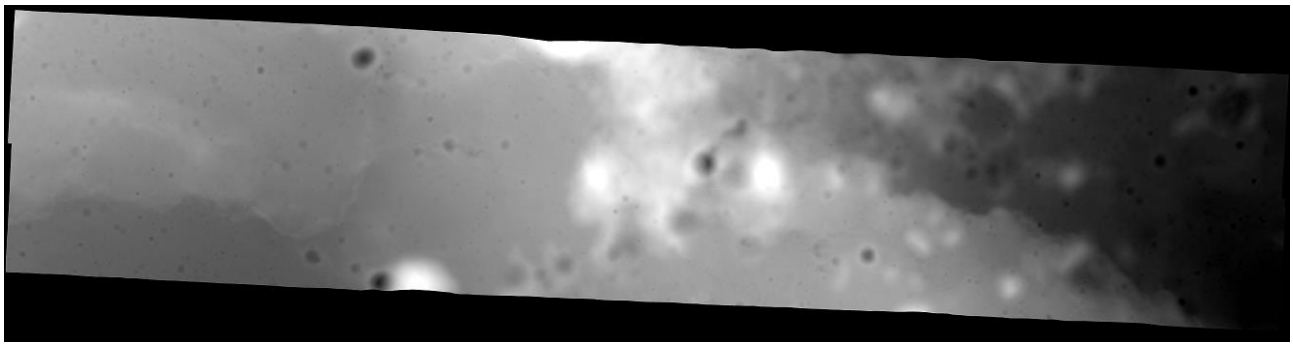

Figure 1: Derived from NAC_DTM_A12LMAS_E039S3387 (rotated 90°)

The PDS DEM was converted to a PANGU DEM stored in PDS single-precision floating point format. This DEM is not unusual in having outer regions of unknown values to fit into a rectangular DEM shape necessary for the PDS (Planetary Data System) format, and in this instance, the unknown values were set to the lowest elevation point to be unobtrusive to the simulation. The DEM was converted to a PANGU model and rendered as shown in Figure 2.

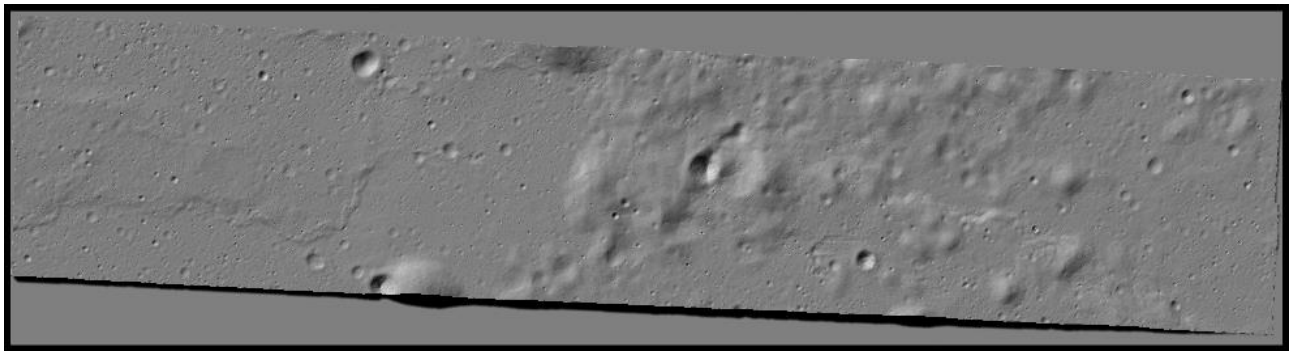

Figure 2: PANGU rendered NAC DEM (rotated 90°)

4.2 PANGU enhanced model

A target landing site and simple approach trajectory from right to left looking from Figure 2 are defined. Resolution enhancement regions are specified in concentric rectangles with resolution jumps of a factor of two between each section to minimise the effect of the resolution change boundary. The high-resolution region is defined in Table 1 and shown graphically in Figure 3, providing a resolution increase from 5m to 0.15625 m in the final region. The resolution increase is obtained through using a variant of mid-point displacement to interpolate the additional sample points with added fractal noise of controllable roughness and amplitude.

Table 1: LROC NAC PANGU region definition

Layer	Centre (m)	Dimension (samples)	Horizonal Resolution (m)
0	n/a	2790 × 10683	5
1	0, 0	3000 × 12000	2.5
2	0, 2000	3000 × 12000	1.25
3	0, 6000	3000 × 3000	0.625
4	0, 6000	3000 × 3000	0.3125
5	0, 6000	3000 × 3000	0.15625

PANGU will use the region definition to generate a multi-resolution model in a bi-tree structure so that each section of increasing resolution is stored in both the original and enhanced resolution enabling PANGU to use depth of view to render each terrain section at the highest appropriate resolution available in the model, while avoiding over rendering artefacts which can occur when the

model resolution is significantly higher than the rendered image pixel resolution. Separate Hapke BRDF materials are applied to the surface and the added boulders which are defined in multiple-resolutions versions in a bi-resolution tree to enable the appropriate resolution to be rendered based on view depth. This approach minimises over-render artefacts and increases rendering performance.

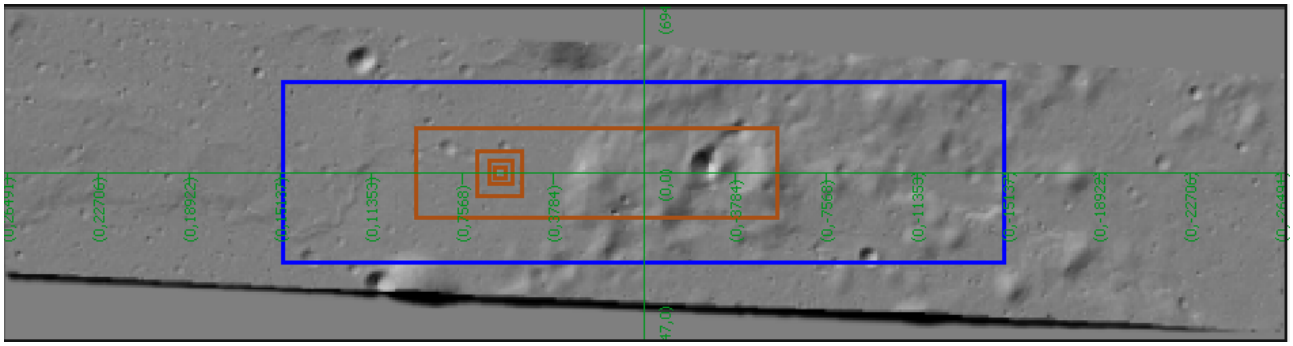

Figure 3: Defining the higher resolution regions (rotated 90°)

A diameter density distribution of small craters less than 20m in diameter (which aren't clearly defined in the 5m DEM) is specified using a standard crater diameter distribution power law to control the crater diameter-density distribution as defined in Eq. 1:

$$N(D) = \mathbf{0.02\ D^{-2.0}} \quad (1)$$

PANGU will use this distribution to generate a probability function which can be sampled with a random generator to generate a representative list of craters to add to the multi-resolution terrain model, with the diameter range appropriate to each higher resolution, ranging from 0.5m to 20m. As boulders are a potential significant hazard for any lander, multiple boulder forms are specified, and a boulder size-density distribution is also defined to generate a list of boulders with varying shapes, to add to the terrain model around the target landing sites, with size varying from 0.5m to 20m.

$$N(B) = \mathbf{0.001\ B^{-3.0}} \quad (2)$$

A PANGU screenshot showing the positions of the synthetic craters and the high-resolution region layers, overlayed on an image representing the base DEM, is shown in Figure 4. PANGU will limit the generation of craters in each layer to a minimum pixel size (e.g., 3 DEM pixels) which avoids craters too small to be defined, so that increasingly higher resolution layers will contain higher resolution craters.

4.3 Descent images

A PANGU 3D model is generated from which multiple images are rendered to simulate descending to the target landing site, and to demonstrate the difference between generating images directly from the original DEM and from the PANGU enhanced model. The top rows of both Figure 5 and Figure 6 show images rendered directly from the base DEM and the bottom rows the equivalent images from the PANGU enhanced model. Figure 6 shows the added synthetic detail and small craters which are defined in the define with insufficient resolution to appear realistic in the rendered images. PANGU includes a facility for replacing craters such as these if they are critical to a simulation but the process is not automated and requires some manual tweaking to achieve good results [9].

An example camera model was defined with an offscreen rendering buffer of 4096×4096 (improves image quality), detector of dimensions of 1280x720 for 720p video with 10-bit ADC (8-bit output), quantum efficiency of 1.0, gain of 5.0, well capacity of 334×10^3 e- and no white noise (this makes

mp4 video encoding difficult for demonstration purposes), an exposure time of 7ms, dark current 4000 e-/pixel/s (~7% level), a small negative/barrel distortion (R^2 coefficient of-6.2147142×10^{-8}) and a camera aperture of 1cm. We also included exaggerated environmental properties with a proton cosmic ray flux of 2×106 and post-processing: gamma correction of 2.4 (sRGB output).

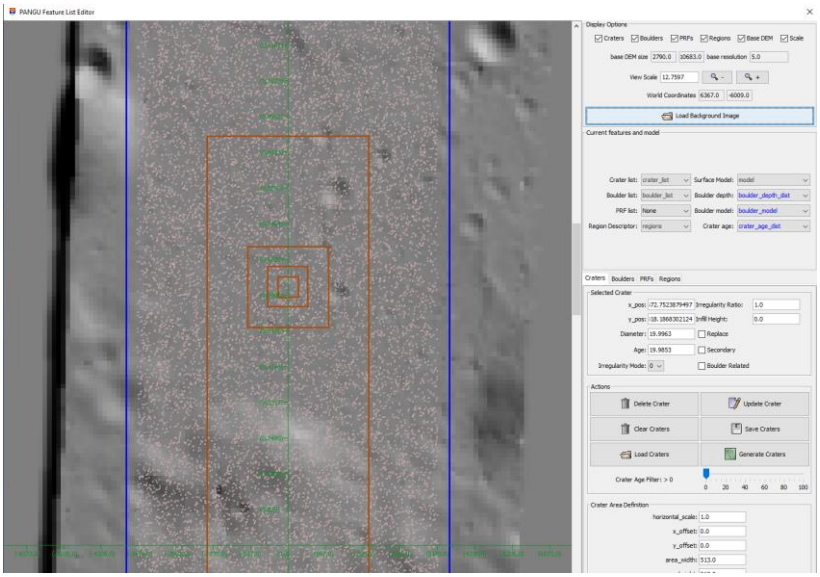

Figure 4: Defining a crater distribution in PANGU

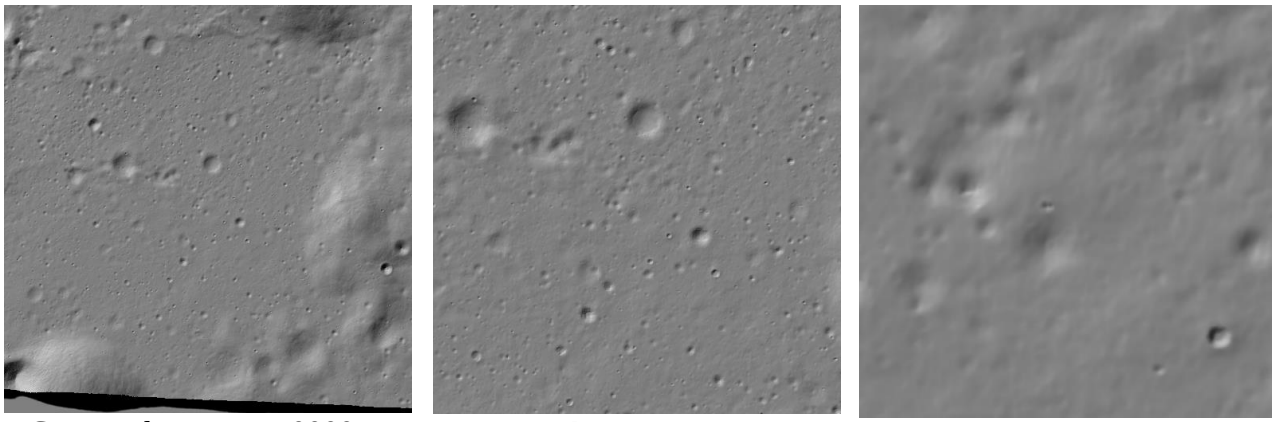

Camera distance = 20000m | Camera distance = 10000m | Camera distance = 2000m

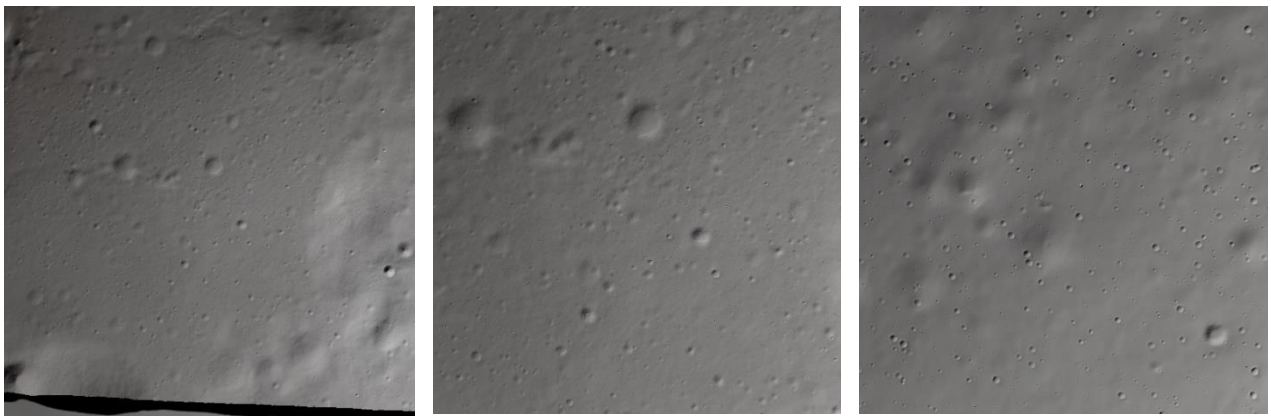

Camera distance = 20000m | Camera distance = 10000m | Camera distance = 2000m

Figure 5: Rendered images from LROC NAC DEM (top row) and from the PANGU enhanced version (bottom row) from a simulated descent sequence.

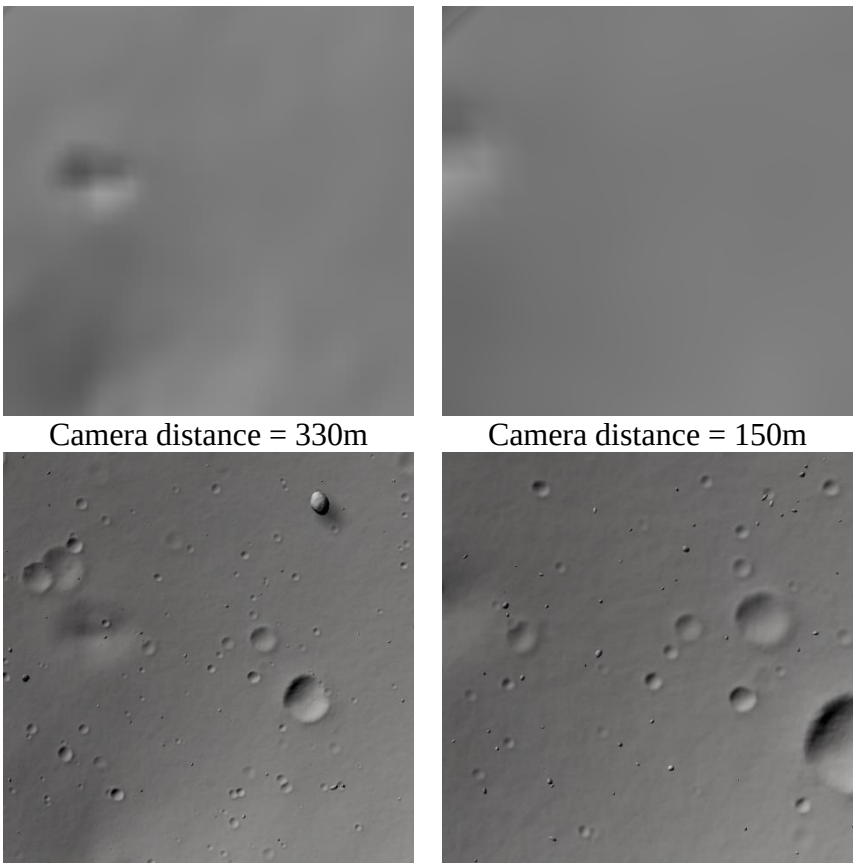

Figure 6: Rendered near surface images from the LROC NAC DEM (top row) and from the PANGU enhanced version (bottom row).

In tests on a standard laptop (Intel Core i7, 16GB memory and GeForce GTX 1050 Ti GPU), frame rates of 2–10Hz were obtained with approximately 150M triangles per second with the default PANGU chunked level of detail setting enabled [2]. The use of a pre-calculated static shadow map has a significant performance enhancement over dynamic shadows which require multiple rendering passes to implement the depth range of shadows required for a descent simulation. The frame rate varies with the number of meshes in view, this is highest when most of the terrain is viewed when far away or close to the surface when many boulders need to be rendered in their higher resolution forms.

4.4 Texture filtering

Texturing in PANGU utilises the standard computer graphics mip-mapping technique to provide appropriately filtered textures at all camera view distances. A mip-map can be considered to be a pyramidal stack of textures in which each successive level having half the resolution as the layer below it e.g. 256×256, 128×128,…,1×1. Each lower resolution level is obtained by averaging each group of 2×2 pixels from the adjacent higher resolution level (known as box filtering). The rendering system selects the level that is best for the current view, blending between levels to provide smooth changes with distances. This system is effective at avoiding aliasing that would result from attempting to render a texture at much higher resolution than the output image can support. However, the texture must be tiled (repeated) across the surface since the texture is almost always much smaller than the area that it needs to cover at high resolution. This causes a “gridding” artefact to be observed when distant textured terrain is viewed e.g., during landing or in low-angle views from a surface rover. This can be seen in the two left images of Figure 8 where there are obvious repeating tiles and lines.

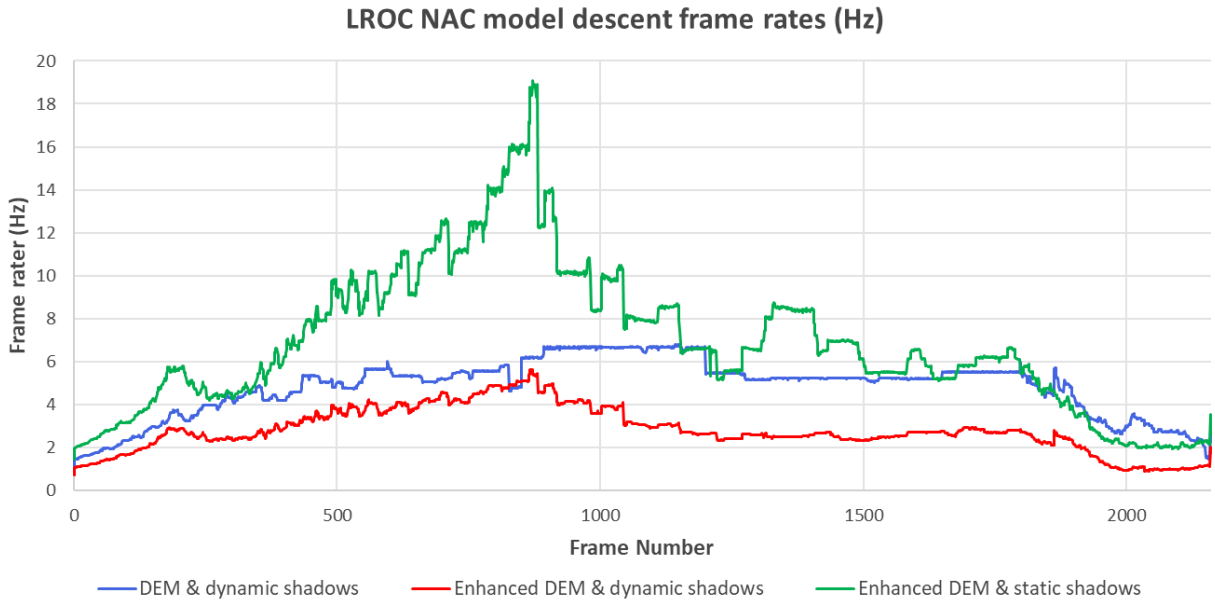

Figure 7: LROC NAC Simulation frame rates

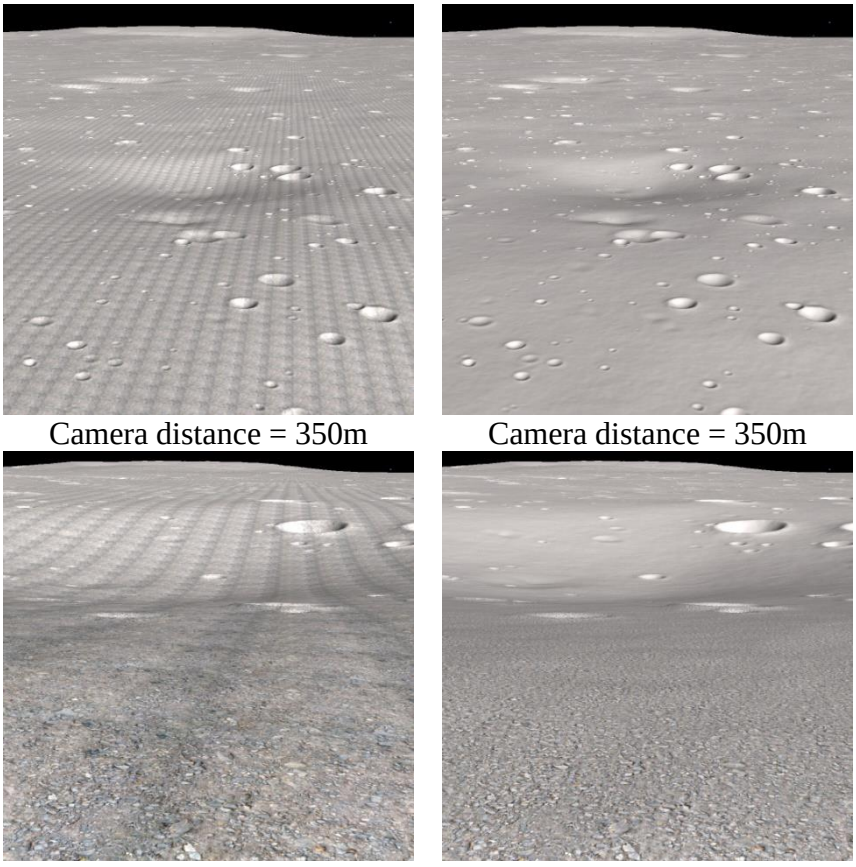

Figure 8: Rendering without (top row) and with (bottom row) texture filtering at different distances.

To avoid the gridding artefacts at large distances, the lowest resolution (lowest spatial frequency) levels of the texture can be filled with the average value. Alternatively, a mip-map pyramid can be constructed in which the pixel values are stored relative to the average value. One of the lower resolution layers, *n-k*, is selected, resized to $2^n \times 2^n$, and then subtracted from the input texture. When the filtered texture is converted to a mip-map by the rendering system, the lower resolution layers

will fade to the average. The parameter k is specified by the user: k=0 corresponds to the average level and has no effect; k=n corresponds to the input texture. Values of about k=4 have been found to work well for textures with dimensions of $2^{10}\times2^{10}$ although it depends on the texture. The benefit can be seen in the images on the right side of Figure 8 with filtering enabled compared to those on the left side without filtering. This texturing approach has the effect of adding surface detail to the model at the highest resolution which then allows a lower mesh resolution than would otherwise be required. However, care must always be taken when using textures to avoid including features that would be too easily detected by feature detecting algorithms.

5 LOW ALTITUDE DESCENT SCENARIO

A different scenario is demonstrated, using the very large combined LRO/Kaguya SLDEM DEM [8] to simulate a low altitude descent trajectory with a swath strip covering half a lunar circumference.

5.1 SLDEM

The SLDEM is imported into PANGU and converted to PDS single precision floating-point format for further processing withing PANGU. DEM sldem2015_128_60s_60n_000_360_float.img was obtained, which covers latitudes of 60S to 60N with a resolution of 128 pixels per degree which is around 60m horizontal resolution at the equator. The DEM has 46080×15360 samples with 32-bit sample resolution in PC_REAL format with a height range of -8717m to 10778m. An image showing this DEM is shown in **Figure 9**. This is a large DEM and converting to a PANGU model results in a model size of approximately 32 GB. To simplify development, the resolution can be reduced by a factor of two during in the import process to obtain a DEM of size of 23040×7680. The resulting PANGU model file is approximately 8GB in size. The higher resolution version is approximately 32GB in size and would require PC memory of ~48GB to run a PANGU simulation.

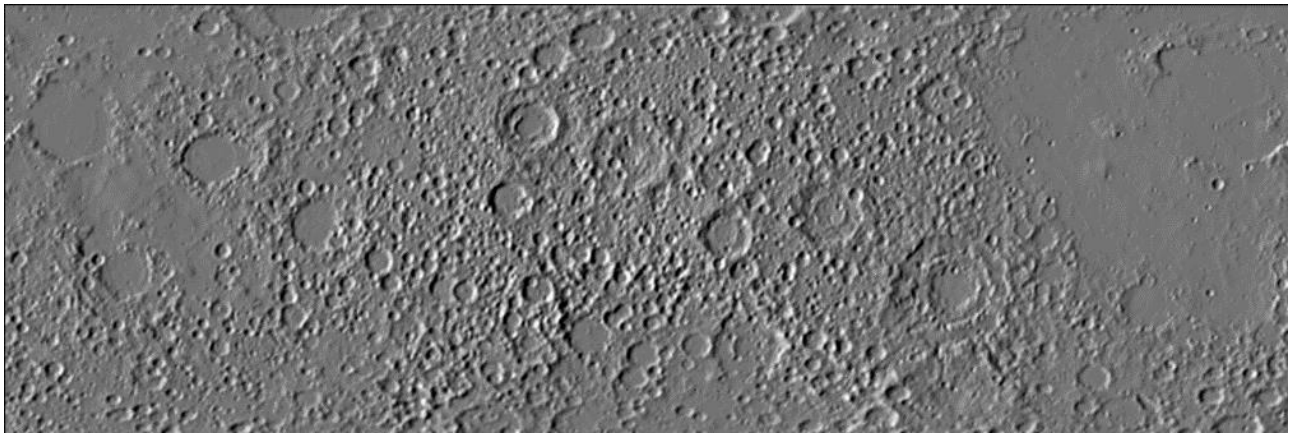

Figure 9: Derived from sldem2015_128_60s_60n_000_360

The approach to create a low-altitude descent scenario based on this DEM is as follows:

- Import the SLDEM into PANGU at different resolutions to allow tests on lower powered PCs as well as high-end ones.
- Define a trajectory flying on a great circle over the middle of the DEM in a PANGU flight-file.
- Define a PANGU regions file (multi-resolution model) to:
    - If memory is an issue, can reduce the resolution of the outer region of the model to reduce memory usage in areas that do not require it for the simulation.
    - Define a high-resolution landing strip towards the end of the trajectory.

- Define camera model parameters to simulate camera distortion.
- Generate the sequence of images from the descent sequence defined in the pre-defined flight-file.

A comparison of the rendering frame rates obtained is given in Figure 11 which shows dynamic shadows versus a predefined static shadow map and including saving or not saving image files, which was included to isolate the rendering frame rate from storing images because a closed loop test could transfer the rendered images through a TCP/IP Socket interface instead of storing to disk. This shows that with dynamic shadows, there was very little difference in the frame rates whether or not the generated images were stored locally, and that 10 Hz was achieved with a static shadow map but that the frame rate then varied between 5-10 Hz when images were stored locally.

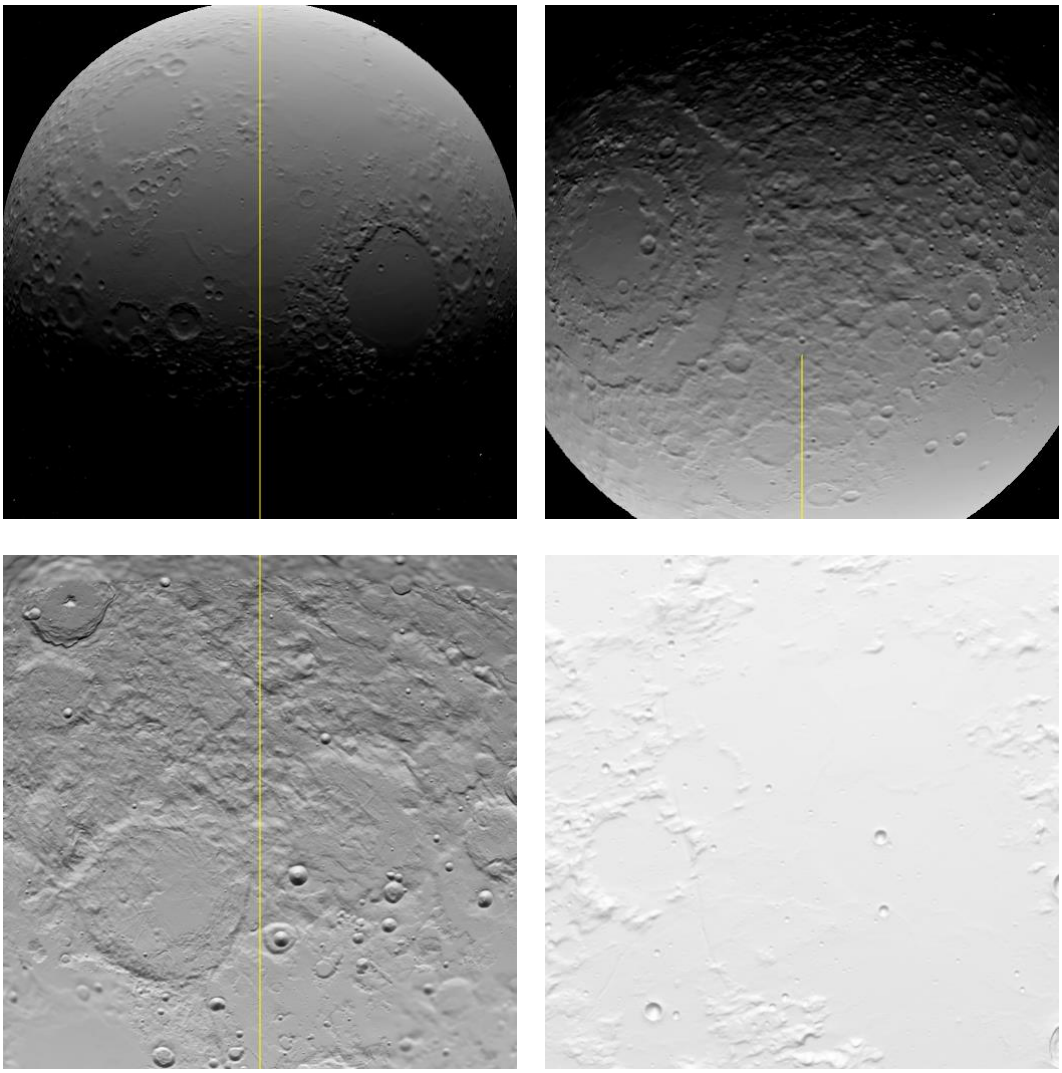

Figure 10: Examples images rendered along the SLDEM lunar descent trajectory

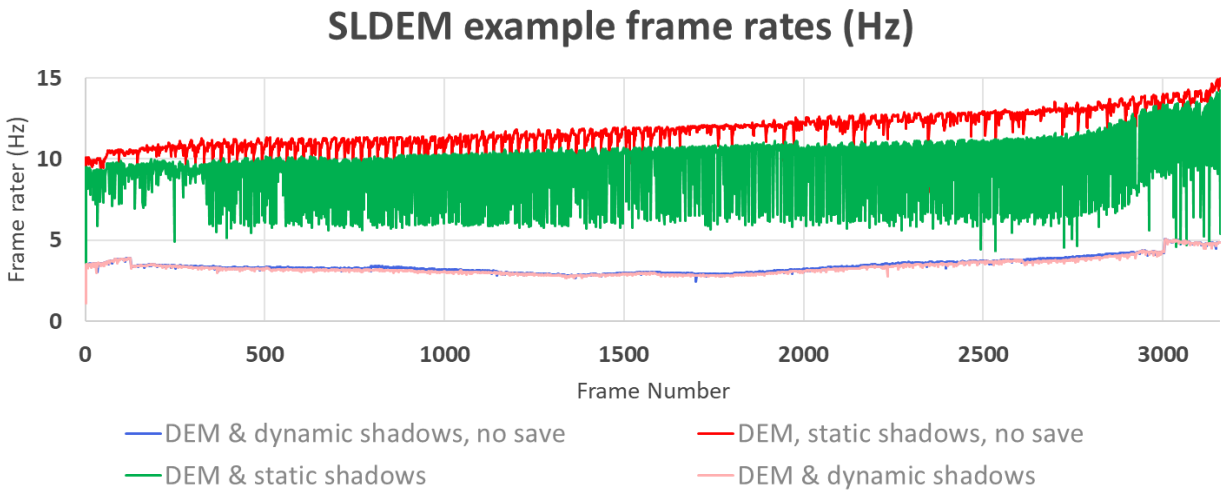

Figure 11: SLDEM example frame rates

6 Conclusions

This paper describes how a range of modelling and rendering features can be used to synthetically enhance the resolution of large and high-resolution DEMs to generate, multi-resolution models suitable for simulating complex GNC scenario, using lunar approach and landing demonstrations. The performance of the LROC NAC model is suitable for closed and hardware-in-the-loop simulations in nominal real-time, but below a nominal 10 Hz real-time target. The larger, SLDEM simulation achieved approximately 10 Hz, but only when a static shadow map was used, and images were not saved locally. However, this shows that large, representative lunar descent examples can be rendered in PANGU in nominal real-time, though some trade-offs in model complexity may be required if 10 Hz is a critical simulation requirement. Options to improve this performance would be to use more powerful hardware, split the model into smaller sections for different stages of the approach and descent or use texturing to simulate surface roughness at the highest resolution and so reduce mesh resolution requirements.

7 Acknowledgements

PANGU and PANGU was developed by the University of Dundee for ESA and is being used on many European activities aimed at producing precise, robust planetary lander and rover guidance systems. This work was carried out under ESA contract number 4000123765/18/NL/CRS/hh.

8 REFERENCES

[1] Dunstan M. and Hornbostel, K., *Image processing chip for relative navigation for lunar landing*, in 9th International ESA Conference on Guidance, Navigation, and Control Systems (GNC 2014), 2014.

[2] Martin, I., Dunstan M. and Sanchez-Gestido M., (2021), *Planetary Surface Image Generation for Testing Future Space Missions with PANGU*, 2nd RPI Space Imaging Workshop, Oct 2021, Saratoga Springs, N.Y, USA.

[3] Woicke S. and Krüger H., *Performance of a Crater Navigation Method for Lunar South Pole Landing*, AIAA 2023-0690, Published Online:19 Jan 2023https://doi.org/10.2514/6.2023-0690.

[4] Smith M., et al. *The Artemis Program: An Overview of NASA's Activities to Return Humans to the Moon* 2020 IEEE Aerospace Conference, Big Sky, MT, USA, 2020, pp. 1-10, doi: 10.1109/AERO47225.2020.9172323.

[5] Fisackerly R., et al., *The ESA Lunar Lander Mission*, Published Online:14 Jun 2012, https://doi.org/10.2514/6.2011-7217 .

[6] Bowler S. (editor), *Why we must go back to the Moon*, Astronomy & Geophysics, Volume 64, Issue 2, April 2023, Pages 2.26–2.29, https://doi.org/10.1093/astrogeo/atad013.

[7] Jonniaux G. and and Gherardi D., *Robust extraction of navigation data from images for planetary approach and landing*, Proceedings of the 9th International ESA conference on Guidance, Navigation and Control Systems, Porto, Portugal, 2014.

[8] Barker M., et al. *A new lunar digital elevation model from the Lunar Orbiter Laser Altimeter and SELENE Terrain Camera*, Icarus 273, pp 346-355, 2016.

[9] Martin I., Dunstan M., Parkes S., and Gestido, M.S., *Testing Vision-based Guidance and Navigation Systems for Entry Descent and Landing Operations*, In IAC 2018 Conference Proceedings (pp. 1-9), 2018, [IAC-18,D1,3,4,x42780].

[10] Martin I., Dunstan M. and Gestido, M.S., *Simulating Infrared Images Of Asteroids And The Lunar Surface In Real-Time For Testing Future Missions*, ESA GNC 2021, Online, June 22nd - June 25th, 2021.

[11] Dunstan M., Martin I., Parkes S. & Gestido, M.S., *PANGU v4: A software tool for testing vision-based guidance and navigation systems for in-orbit, entry descent and landing and surface mobility operations*, DASIA 2018, 29th-31st May 2018 Oxford, UK.

[12] Brochard R., et al. *Scientific image rendering for space scenes with the SurRender software*, 2018, https://doi.org/10.48550/arXiv.2106.11322.

[13] Pajusalu M, et al. *SISPO: Space Imaging Simulator for Proximity Operations*, PLOS ONE 17(3): e0263882. https://doi.org/10.1371/journal.pone.0263882.

[14] Barker M.K., Mazarico, E.M. and Restrepo C.I., *Topographic Models from the Lunar Orbiter Laser Altimeter (LOLA) in Support of Terrain Relative Navigation at the Moon*, Paper SIW22–23, 3rd Space Imaging Workshop, Atlanta, USA, Oct 2023.

[15] Burns, K.N. et al., *Digital elevation models and derived products from LROC NAC stereo observations*, International Archives of the Photogrammetry, Remote Sensing and Spatial Information Sciences - ISPRS Archives. 39. 483-488. 10.5194/isprsarchives-XXXIX-B4-483-2012.